Thermal Plasma in a Rotary Kiln for Cement Production

An Investigation of the Heat Transfer Mechanisms

Master's thesis in Sustainable Energy Systems

JOHN PETERSSON

MASTER'S THESIS 2022

Thermal Plasma in a Rotary Kiln for Cement Production

An investigation of the Heat Transfer Mechanisms

JOHN PETERSSON

CHALMERS
UNIVERSITY OF TECHNOLOGY

Department of Space, Earth and Environment
Division of Energy Technology
CHALMERS UNIVERSITY OF TECHNOLOGY
Gothenburg, Sweden 2022

Thermal Plasma in a Rotary Kiln for Cement Production
An Investigation of the Heat Transfer Mechanisms
JOHN PETERSSON

Thermal Plasma in a Rotary Kiln for Cement Production
An Investigation of the Heat Transfer Mechanisms
JOHN PETERSSON
Department of Space, Earth and Environment
Chalmers University of Technology

Abstract

Due to the urgent global climate challenges, goals have been set by governments and companies in order to reduce their greenhouse gas emissions and their impacts on the climate. This master thesis work examines how the emissions can be reduced for the cement industry, by replacing the heat source in the rotary kiln from fossil fuels with an electrically generated plasma. The possibility of switching the heat source is studied through simulations, in Matlab, using a model which has been previously developed at the division of Energy Technology at Chalmers University of Technology.

The main focus of this thesis is to examine how the heat transfer is affected from using a thermal plasma in the rotary kiln, and to compare the results to a coal flame. The thesis will also focus on examining how the desired product temperatures for the bed material is reached within the rotary kiln. Moreover, how the heat transfer is affected by varying certain process parameters as well as a sensitivity analysis, to investigate the effects of uncertainties, will also be assessed in the thesis.

The simulations indicate a good potential for the implementation of a thermal plasma in the rotary kiln. Increased temperatures in the plasma and the addition of particles to the kiln, showed the biggest impact on the bed temperature, while simultaneously keeping a smooth bed temperature profile.

To improve the simulations and make them more trustworthy, measurements on pilot scaled or full scaled kilns would provide valuable insight. For example, if measurements were to be made on the temperature profile of the plasma, which have been estimated in the simulations in this thesis work, more accurate simulations could be obtained.

Acknowledgements

A huge thank you is directed to the people who have helped me create this thesis. I want to especially thank my examiner and supervisor, at the division of Energy Technology at Chalmers, Klas Andersson and Adrian Gunnarsson for their amazing encouragement and support. I also want to thank the people at Cementa for valuable feedback and a special thank you to Bodil Wilhelmsson and Johan Larsson for letting me attend your weekly meetings and the interest you have shown in my thesis.

Lastly, I want to thank my friends and family for their support and interest in the project. A massive thank you to Amanda for cheering me on!

John Petersson, Gothenburg, May 2022

Contents

Contents

List of Figures

List of Tables

1

Introduction

The current situation regarding an alarming climate change requires that industries, especially large industries, change their present way of operation to a less emission intensive production, with a completely new mindset where the environment is a major priority. For some of these industries, substituting combustion of fossil fuels for electrically generated plasma from renewable resources could be an option. In this thesis, the effects of such a transition will be examined for the cement production process with focus on the heat transfer in the rotary kiln process step, by utilizing a modeling tool and by performing sensitivity analyzes. A few different selected alternatives of operation with a plasma torch will be evaluated during the project.

1.1 Background

Society has some great challenges ahead in order to reduce and limit global emissions of greenhouse gases to be able to meet the 1.5 degree target set in the Paris agreement [1]. Large industries make up a significant portion of these emissions which needs to be reduced. Among others, the cement industry is a major contributor of greenhouse gas emissions and it has currently been estimated that the global cement industry emits about 5-7% of the total CO_2 emissions worldwide [2]. Globally, one ton of cement emits 0.59 tons of CO_2 [3]. The possibility to limit the emissions from cement industry would thus, have a major impact on the total emissions [2]. Furthermore, the use of cement is not predicted to decline in the upcoming years, but rather increase, why it is of great importance to focus on the emissions from the cement process [4]. Cementa, which is the largest producer of cement in Sweden, whom's process will be studied in this project, has a vision to be carbon neutral in 2030 [5]. The goal is ambitious and requires some dramatic changes to their present operation of their production in order to succeed.

To produce cement from limestone, there are currently two process steps in which the majority of carbon dioxide emissions occur, from the calcination reaction, which can be seen in Reaction 1.1, and from the fuel combustion in the calciner and the rotary kiln [6].

$$CaCO_{3(s)} \rightarrow CaO_{(s)} + CO_{2(g)} \tag{1.1}$$
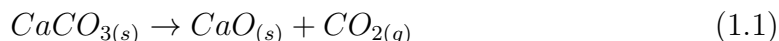
In the calcination step, the reaction caused by heating the raw material decomposes the calcium carbonate and forms calcium oxide and carbon dioxide, and the emission can thus not be avoided. However, using carbon capture and storage (CCS) technologies for this process step has been suggested as a solution to prevent emissions to the atmosphere [7]. While CCS could also be used to reduce emissions

related to the combustion within the process, one interesting suggested method for Cementa's process is to replace the current fossil fuels used in the burners to heat up the material of the process with an electrically generated plasma. By using electricity generated from renewable resources, such as solar or wind power for example, the emissions from this step in the process could be significantly reduced. In this thesis, the working gas considered to be used for the plasma torch is CO_2, since it can be gathered from the calcination process previously mentioned and because CO_2 has good radiative properties. Utilizing this residual gas stream could potentially also be an economically favourable option, since the gas could be considered "free of charge". However, the heat transfer properties from the plasma torches will differ in comparison to the flame generated by the current fossil fuels. The plasma torches will have a substantially higher maximum temperature than the current flame, and the plasma will probably have a smaller diameter and is thus more concentrated [8]. Furthermore, the plasma does not contain any soot, ash or carbon particles, which normally both emit and absorbs radiation [9]. The effects theses changes may have on the heat transfer to the cement bed is essential to understand before an implementation is possible.

Therefore, creating realistic simulations is a great step towards understanding and estimating what is happening inside the closed process and gives a solid foundation for decisions about operation and future investments.

1.2 Aim of study

The aim with this master thesis work is to examine how changing the heating source in a rotary kiln from combustion of fossil fuels to using an electrically generated plasma will affect the bed material and thereby the cement production. Also, the project will cover development of a modelling tool and a sensitivity analysis where it will be investigated how the heat transfer vary with certain parameters. The potential outcome of the study is a better understanding of the heat transfer in rotary kilns for industrial processes, such as for the cement industry. Additionally, this study aims to give potential recommendations of process changes that could be beneficial if implemented, or recommendations regarding the conditions of the process.

1.3 Limitations

The only process that will be considered in this study is the process for cement production at Cementa. Moreover, only the heat transfer in the rotary kiln will be investigated in detail and the entire process will thus not be discussed in depth. Furthermore, a limitation to the development of the model is that there is at this current time no cement process at full scale which operates with a thermal plasma, the model can therefore not be fully validated. Also, it has proven difficult to perform measurements on the actual process at Cementa, in Slite, due to the fact that the rotary kiln is 80 meters long without windows or access points for measurements [10]. However, the model could be verified in an earlier step by performing exper-

iments and measurements on a pilot scale kiln rather than on the actual capacity of the process. Though, such measurements are not included in this thesis work. Additionally, the implementation of CCS will not be discussed further than that it would be necessary as a means to remove all emissions from the process.

1.4   Specification of issue

The heat transfer model used in this master thesis work has previously been developed at the division of Energy Technology at Chalmers University of Technology, and has been verified with measurements from experiments and from operational data at an industrial scale, for the combustion of fossil fuels in a rotary kiln. Now, if the current heat source of fossil fuels are to be replaced by an electrically generated plasma for the cement industry, the model needs to be altered to fit the characteristics of a thermal plasma. As opposed to the flame generated by fossil fuels, the plasma torch has a higher maximum temperature and a smaller diameter. Due to the closed structure of the kiln and its length, it is difficult to measure the effects of the flame on the cement bed in the middle of the kiln. Also, due to the large capacity and thus, high investment costs, it is beneficial and cost effective to first develop a model to verify, or give an indication, of whether it is possible or not to make the transition to thermal plasma.

2

Theory

In the following sections, relevant theory is presented to provide information about the studied process and it's key components as well as the plasma torch and the modelling tool used in this work. General information is provided and more detailed information about the specifics of the process studied during this thesis is presented in chapter 3.

2.1 Cement process

This section will describe a general cement production process, where the main process steps are illustrated in Figure 2.1, further details about the specifics at Cementa's site on Gotland will be presented in chapter 3.
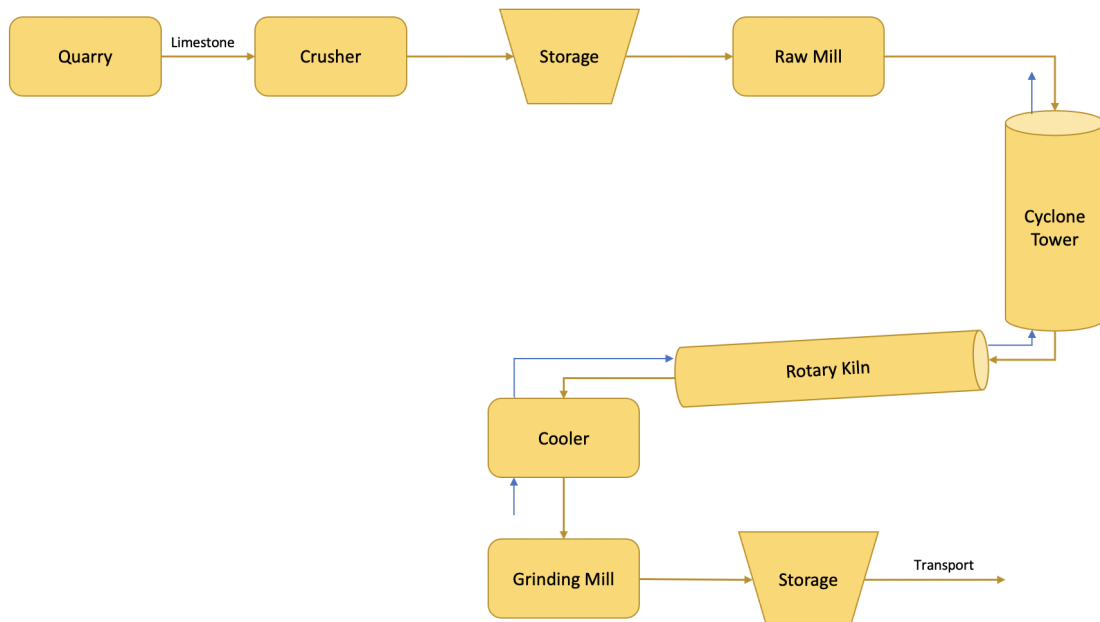
Figure 2.1: A basic schematic over a general cement production process. The shapes represent the different process steps, the yellow arrows the flow of the material and the blue arrows indicate the flow of gas.

The process begins with the extraction of raw material, which occurs in deposits such as quarries or mines, where limestone, marl or chalk is extracted as a source of

calcium carbonate (CaCO₃) [11][12]. Small amounts of iron ore, shale, bauxite, clay or sand can be used as an additive to provide aluminum oxide (Al_2CO_3) and silicon dioxide (SiO_2) to alter the composition of the raw meal to meet the requirements on the product [11]. The raw materials are then ground to a fine powder to achieve a quite narrow size distribution of the particle feed to increase the reaction rate of the calcination and clinkerization reactions due to an improved contact between particles and hot gases [11]. Furthermore, to reduce the variability of the raw meal, silos are used to mix the material to create a homogeneous raw meal [11]. Also, the silos provide the possibility to store the meal to allow for a continuous flow of meal even if there has not been any new raw materials extracted recently [13]. A typical mixture of raw meal contains approximately 75-80 wt % limestone and 20-25 wt % clay, as well as smaller amounts of iron ore and sand to regulate the composition of materials required to meet certain product specification [13]. After the silos, the ground raw meal is fed to a sequence of cyclones, acting as a heat exchanger, where the meal is preheated with hot flue gases from the downstream combustion in the process [11]. Depending on the moisture content of the material, the amount of cyclones can differ between different sites and processes with up to six cyclone stages [11]. As the raw meal has been dried and heated, the calcination process begins, in which the meal has achieved a temperature around 800°C [13]. The main part of the calcination, reaction 2.1, occurs in what is called the calciner, where the calcium carbonate is decomposed to calcium oxide and carbon dioxide [13]. Due to the reaction being endothermic, heat is supplied to the calciner through combustion as well as by flue gases from the downstream rotary kiln, this is an energy intensive step of the process, which consumes about 60% of the required total energy of the plant [13].

$$CaCO_{3(s)} \rightarrow CaO_{(s)} + CO_{2(g)} \tag{2.1}$$
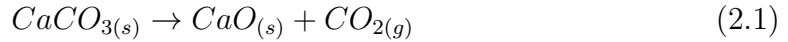
Thereafter, the hot calcinated meal continues by entering a rotary kiln, which is a long rotating furnace that is refractory lined with an outer steel shell. In the kiln the meal is heated by a large flame with the burner located at the outlet of the kiln, and further reactions occur in the bed of meal at a higher bed material temperature of up to 1450°C [13]. The main reactions taking place in the rotary kiln, called clinker reactions, are presented in reactions 2.2 to 2.5 [13]

$$2CaO_{(s)} + SiO_{2(s)} \rightarrow Ca_2SiO_{4(s)} \tag{2.2}$$

$$CaO_{(s)} + Ca_2SiO_{4(s)} \rightarrow Ca_3SiO_{5(s)} \tag{2.3}$$

$$3CaO_{(s)} + Al_2O_{3(l)} \rightarrow Ca_3Al_2O_{6(s)} \tag{2.4}$$

$$4CaO_{(s)} + Al_2O_{3(l)} + Fe_2O_{3(l)} \rightarrow 2Ca_2FeAlO_{5(s)} \tag{2.5}$$
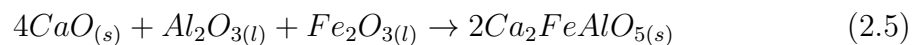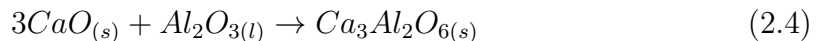
Furthermore, the rotary kiln rotates at a constant speed which helps create lumps, or nodules, of clinker besides also transporting the product towards the end of the kiln due to the slight inclination, which is between 1° and 3° [13]. A rotary kiln is

used in this process step with advantage since it allows for good contact between the reacting solid compounds as the bed is continuously mixed, moving from the higher to the lower end of the kiln. The rotary kiln is explained in further detail in section 2.2.

After the rotary kiln, the product, which is now considered to be cement, quickly needs to be cooled, in order to stabilize and prevent backwards reactions, where the desired product alite (Ca_3SiO_5) partially could transform back to calcium oxide and belite (Ca_2SiO_4) [13]. This takes place in a grate cooler, where cool air recovers the heat from the hot cement while simultaneously stabilizing the product [13]. The air that cools the product goes through the kiln and is further used to preheat the meal in the cyclones and also used to provide heat in the calcination step.

Due to a wide size distribution of the product leaving the cooler, the cement is further ground, in a mill, after the cooling process to achieve more equal particle sizes [13]. During this process step, 3-6 wt % gypsum as well as other substances, is also added to the product mixture to improve the strength and setting of the product [13]. Furthermore, ashes formed during the combustion of solid fuels are added to the final product, based on the composition of the raw materials used [13]. After this process step, the product is finalized, and may be stored in silos before being delivered to costumers [13].

2.2 The rotary kiln

The kiln, in which complex solid-solid reactions of the system occurs, is a cylindrical tube between 40-100 meters long [13]. The materials which are heated inside the kiln are transferred along the axis by a slight inclination and a continuous rotation of the cylinder. The tube itself, consist of a steel outer shell and a protective inner layer to shield the tube from the high temperatures generated by the flame [13]. Bricks are commonly used to provide the protection and insulation required for the steel shell of the kiln. However, cement clinker will eventually stick to the bricks on the inner kiln wall, and over time some of the bricks are pulled off and becomes part of the product mixture [13]. This causes that the process must be stopped about once a year for maintenance, to remove the build up of clinker on the wall and to reline the refractory [13].

To supply the required energy for the clinker reactions to occur, there is a burner located at the bed material outlet of the kiln [13]. It is common that solid fuels are used for the burner, which provides particles, which can help transfer heat to the bed of the kiln through radiation [9]. In Figure 2.2, courtesy of Adrian Gunnarsson, a visualisation of a rotary kiln can be seen [9].
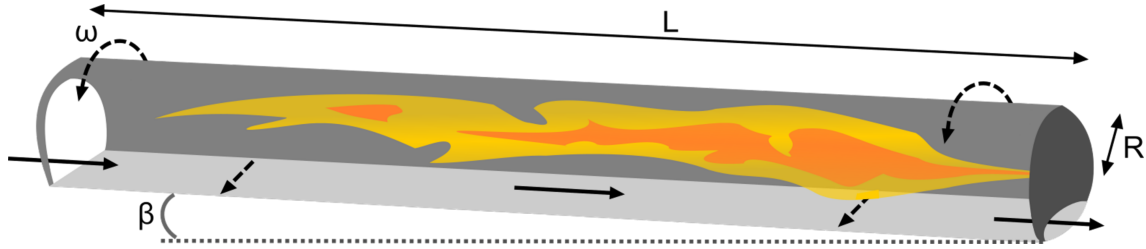
Figure 2.2: A visualisation of the rotary kiln with a bed material, arrows indicating motion of bed and kiln as well as length, radius and angle of incline [9]

2.3 Plasma torches

Thermal plasma's can be characterized by high temperatures, ranging from 2000-20000°C [8], and the ability to convert electrical energy into thermal energy. This is achieved by establishing an electric arc between an anode and a cathode within the plasma device, which is called a plasma torch, while simultaneously having a continuous flow of gas [14]. In Figure 2.3, courtesy of Rudolfensis, a simple schematic of the cross section of a non-transferred DC plasma, which is the type of plasma studied in this master thesis, can be seen [15].
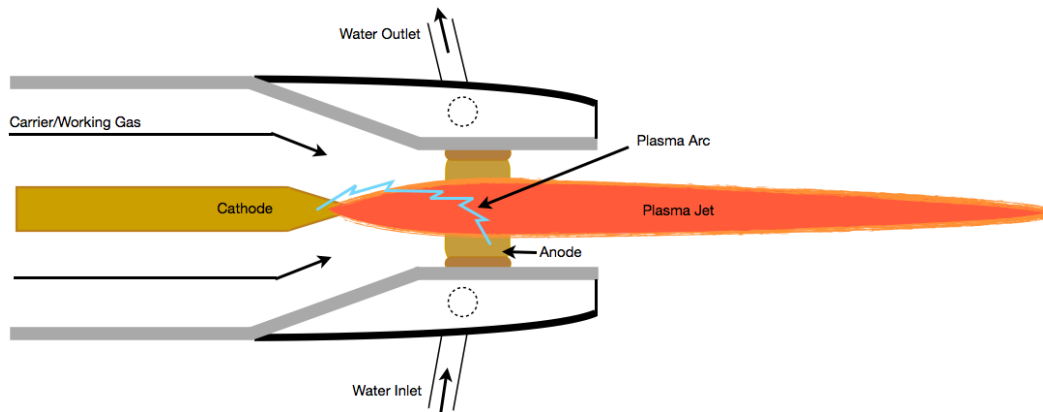
Figure 2.3: Schematic of a cross section of a non-transferred DC plasma with its various components and flows [15]

Moreover, the electrodes are divided by insulation, which contains an inlet for the working gas [8]. The continuous flow of gas stabilizes the arc, which keeps the arc at steady state. In other words, the flow of gas defines a path for the electric arc by cooling the outer layers [8]. The electric arc itself, is established by a continuous discharge of electrons, through thermionic emission, from the cathode. Furthermore, the electric arc can be considered quasi-neutral, since the electrons originate from neutral particles, which means that roughly the same amount of ions and electrons exist in the arc simultaneously [16]. The choice of gas used within the plasma, called the working gas, is mainly based on cost, enthalpy and reactivity [8]. Some examples of gases that are regularly used for plasmas are argon, hydrogen, helium, nitrogen

and air [8]. However, for the cement process studied in this work, the intended gas is carbon dioxide since it is emitted during the calcination step of the process and is thus a viable option, both considering economical and practical reasons. The working gas becomes partially ionized as well as electrically conductive, when flowing through the electrical arc [14]. Although only a small portion of the gas itself reaches the plasma state, the rest of the gas is heated by this small portion of gas [17]. The plasma torch forms a high temperature beam in it's core, but which rapidly decreases in temperature in the peripheral direction [16]. Due to the high temperatures at the electrodes, water cooling is supplied to prevent the electrodes from wearing out too quickly [17].

An equilibrium or thermal plasma reaches a local thermodynamic equilibrium where the ions and electrons are at similar temperatures, as opposed to non-equilibrium or cold plasma, where the temperatures differ between the ions and the electrons [14]. These two variants of plasma have individual properties and different applications. The different variants of plasma's can be further classified based on their design. There are non-transferred and transferred arc mode plasma's, where in the former the two electrodes are contained within the torch, while in the latter the electric arc is established between the cathode within the torch and the anode outside the torch [14]. In this thesis, a thermal non-transferred arc mode plasma is examined as the heating source for the rotary kiln.

2.4 Implementation of plasma torches in the cement process

As mentioned previously, carbon dioxide is released during the calcination step of the cement production process. Thus, there exists an opportunity to capture the carbon dioxide released in the calcination step and utilizing the gas as the fuel for the plasma torch. Furthermore, the plasma could then potentially replace the fossil fueled burner in the rotary kiln. This would, however, change some of the process conditions. The gas inside the kiln, which normally is air mixed with flue gases would be replaced by pure carbon dioxide. The calcination and possibly other reactions are also affected by the change from air to carbon dioxide by increased reaction temperatures. The exchange would further affect the radiation from the flame/plasma, since no radiating particles or water would be present in the flame or gas volume but only carbon dioxide. However, carbon dioxide also radiates heat which makes it a good option for radiative heat transfer.

Furthermore, a completely sealed process, without leakage, is desirable to achieve a pure carbon dioxide outlet stream from the process to minimize the energy required for separation before the carbon dioxide can be stored by applying CCS and thereby remove emissions to the atmosphere from the cement production. It is however, probably impossible to completely remove all leakages, but a high purity of carbon dioxide is still valuable, which should be possible to achieve.

To adapt the process to the changes caused by implementing a plasma, remodelling of the process might be necessary, by for example using a smaller kiln or several plasma torches. However, in this thesis work the current dimensions of the rotary

kiln will be considered, to examine what would be required from the plasma generator.

2.5 Heat transfer modelling in a rotary kiln

Inside the rotary kiln, the heat is transferred through four major mechanism. These mechanism are radiation, convection, conduction as well as heat generated from the occurring reactions. Radiation is transferred from the flame to the wall as well as to the bed, furthermore, the walls transfer heat through radiation to other wall surfaces and to the bed. Moreover, heat is transferred to the wall and bed through convection from the gas inside the kiln, as well as to the surrounding air outside the kiln. Heat is also transferred by conduction from the wall to the bed where they are in contact, in addition to through the wall to the outside surface of the kiln. Additionally, heat is consumed during the reactions taking place inside the kiln. However, with the high temperature conditions within the kiln, radiation come to dominate the total heat transfer to the bed material.

Since the kiln rotates, the bed is heated in different ways depending on where it is located. The bed can be considered to be divided into two layers, one top layer which is heated by radiation and convection, and one bottom layer which is in contact with the hot wall and thus heated through conduction [9]. These two layers are moving in opposite directions since the bottom layer is considered to follow the direction of the moving wall until it reaches the top of the bed and starts rolling down the bed, see Figure 2.4, courtesy of Adrian Gunnarsson [9].
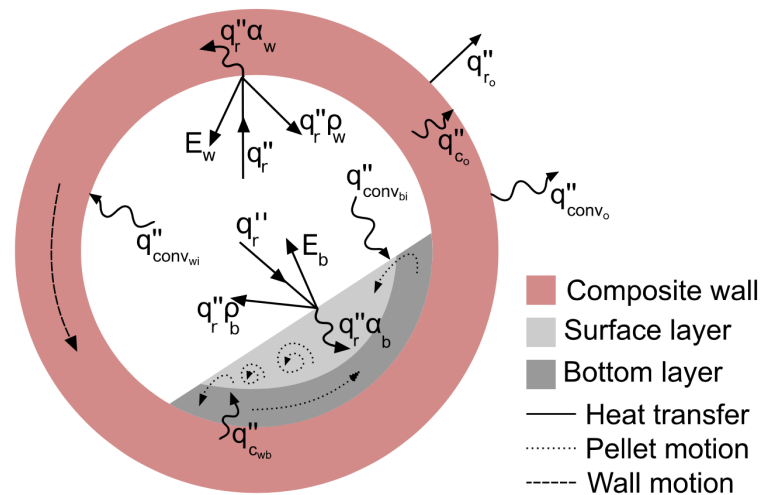
Figure 2.4: Cross-section of a rotary kiln with different heat transfer mechanisms and motions of the wall and pellets [9]

To solve these heat transfer phenomenon, a heat transfer model has been developed in Matlab at the division of Energy Technology at Chalmers University of Technology. A complete description of the model can be seen in the work by Gunnarsson et al. [18]. The model divides the kiln in a set number of cells in radial, axial and

angular directions and solves the heat transfer equations in an iterative manner. The model starts with solving the radiative heat transfer equation (RTE), which can be seen in equation 2.6, in all cells for the initial intensities. The RTE is solved using a discrete ordinates method in which a set number of directions and weights are used to calculate rays of intensities and through inputs such as temperature, gas composition and particle properties the model can calculate radiative intensities and radiative heat flux [9].

$$\frac{dI_\nu}{ds} = \kappa_\nu I_{b\nu} - (\kappa_\nu + \sigma_{s\nu})I_\nu + \frac{\sigma_{s\nu}}{4\pi}\int_0^{4\pi} I_\nu(\hat{s}_i)\Phi_\nu(\hat{s}_i,\hat{s})d\Omega_i \tag{2.6}$$

In equation 2.6 I is the intensity, ν a given wave number, κ is the absorption coefficient, σ_s the scattering coefficient, $\hat{s}_i$ is a direction from which intensity is being scattered, $d\Omega_i$ is the solid angle of the ray in the direction $\hat{s}_i$. Furthermore, Φ_ν is the scattering phase function which is the probability that a ray in the $\hat{s}_i$ direction is scattered in the $\hat{s}$ direction.

The heat transfer through conduction, which occurs between the bed and wall beneath the bed, is calculated using an unsteady-state penetration model as heat is transferred for a certain time as the bed travels with the wall [9]. Furthermore, the model assumes a no-slip condition between the bottom of the bed and the wall, as well as a no mixing assumption of the bottom layer [9]. Equation 2.7 is used to calculate the temperature of both the bed and wall at its contact point.

$$T_{cs} = \frac{(k\rho C_p)_w^{0.5}T_w + (k\rho C_p)_b^{0.5}T_b}{(k\rho C_p)_w^{0.5} + (k\rho C_p)_b^{0.5}} \tag{2.7}$$

In equation 2.7 T_{cs} is the contact surface temperature, k is the thermal conductivity, ρ is the density, C_p is the specific heat capacity and T is the temperature. The indices w and b imply wall and bed respectively. As a consequence of that the bed and wall are only in contact for a certain period of time and due to the dependency of the rotational speed and to what degree the kiln is filled with bed material, steady state can not be assumed. Thus, an unsteady-state penetration model is used and the heat transfer between the bed and the wall can be described by the following equation [9].

$$W_{cond,b/w} = A_w X_c \left[\rho C_p \int_0^{t_{\Psi b}} \int_{d_T=0}^{d_T=0.99} \delta T(\delta,t)d\delta dt\right]_{b/w} \tag{2.8}$$

In equation 2.8 W is the accumulated heat, A is the surface area, X is the volume portion of the bed consisting of solid material, $t_{\Psi b}$ is the period of time the bed is in contact with the wall before it reaches the top and starts to fall down, δ is the thermal penetration depth which is calculated by equation 2.10, d_T is the temperature distribution within the thermal penetration depth of the wall or bed which is calculated by equation 2.9 [9].

$$d_T = \left[\frac{T(\delta,t) - T_{cs}}{T_i - T_{cs}}\right]_{b/w} = \left[erf\left(\frac{\delta}{2}\left(\frac{kt_\Psi}{\rho C_p}\right)^{-0.5}\right)\right]_{b/w} \tag{2.9}$$

$$\delta_{b/w} = 3.64 \left[\sqrt{\frac{kt_\Psi}{\rho C_p}} \right]_{b/w} \quad \text{(for } d_T = 0.99) \tag{2.10}$$

The convective heat transfer, which occurs between the gas and the bed/walls in the kiln, due to the temperature difference between the bed/walls and nearby gas, must also be considered. This is done through equations 2.11 and 2.12 respectively, which describes the heat transfer coefficients [9].

$$h_{g \to w} = 0.036 \frac{k_g}{D} Re_D^{0.8} Pr^{0.33} \left(\frac{D}{L} \right)^{0.055} \tag{2.11}$$

$$h_{g \to b} = 0.4 G_g^{0.62} \tag{2.12}$$

In the two equations above, h is the heat transfer coefficient, D is the diameter, Re is the Reynolds number, Pr is the Prandtl number, L is the kiln length, G_g is the gas mass flux and the indices g and w are short for gas and wall respectively. Additionally, to account for the heat losses from the kiln, heat is transferred through the wall of the kiln to the outside where the heat is lost to the surroundings through both radiation and convection. An expression for the outer wall temperature T_{w_o}, seen in equation 2.13, can then be obtained [9].

$$T_{w_o} = T_{w_i} - \frac{T_{w_i} - T_\infty \cdot \frac{ln\left(\frac{D_o}{D_i} \right)}{k_w}}{\frac{ln\left(\frac{D_o}{D_i} \right)}{k_w} + \frac{1}{D_o/2} \left(\frac{1}{h_o} + \frac{1}{\epsilon_{wo} \sigma (T_{wo} + T_\infty)(T_{wo}^2 - T_\infty^2)} \right)} \tag{2.13}$$

In the equation above, ϵ is the emissivity coefficient and σ is the Stefan-Boltzmann constant. The convective heat transfer coefficient of the outer wall is calculated with equation 2.14, which is a correlation for rotating, horizontal cylinders [9].

$$h_o = \frac{k_{go}}{D_o} 0.11 [(0.5 Re_\omega^2 + Gr_o) Pr_o]^{0.35} \tag{2.14}$$

Gr in the equation above is the Grashof number.

3

Method

This master thesis work will be a continuation and be based on previous modelling work, done in collaboration with Cementa, to provide an improved understanding of the heat transfer phenomenon in rotary kilns and how the process can be adapted to use plasma as a heating source. This thesis work began with a literature study where information about rotary kilns, thermal plasmas, the process at Cementa and the already existing model tool was gathered. This was done to achieve an increased understanding about the subject and how to proceed with the different cases which were to be modelled. A reference case, both for a coal flame and a plasma, was established, which contains a first set of parameters to model. The reference case model was used as a benchmark to be compared to the cases which are simulated at a later occasion. Both during and after the reference case was modelled, some model development, which was an iterative process, took place in order to improve and adapt the model to a plasma flame. This included gathering knowledge, through literature, about how a plasma differs from the regular fossil fueled combustion. Subsequently, several different interesting cases based on literature, previous experiments, qualitative guesses, and the results from the reference case were simulated and a sensitivity analysis was performed. An optimization process of the model was also performed and recommendations regarding how to run the kiln for an optimal heat transfer performance were derived as a last step. Additionally, the results from the simulations were documented during the entire course of the project.

The reference case simulations have many similarities with the actual process with regards to process conditions and dimensions. This was done in order to investigate if it would be viable to change as little as possible in the current process to make the transition towards using plasma torches easier. Therefore, the dimensions were kept the same and the flame was simply replaced with a plasma of pure CO_2. Several simulations were made to see how parameters such as the temperature of the plasma jet and the inlet gas temperature affected the temperature of the bed at the outlet of the kiln. Furthermore, simulations were performed with a certain amount of particles present in the kiln to investigate how different amounts of particles affected the radiation.

The desired results from the simulations is a bed material temperature, at the outlet of the kiln, of 1450°C with a relatively smooth temperature profile throughout the kiln.

3.1 Reference case

In Figure 3.1, courtesy of Cementa, a schematic of the cyclone tower, rotary kiln, and cooler can be seen with the material flow and gas flows indicated by colored arrows. At Cementa's site on Slite, the rotary kiln has a length of 80 meters and an inner radius of 2.1 meters, these values have been kept constant through-out all the modelled cases. Furthermore, the gas flow rate in the kiln, called secondary air in Figure 3.1 was kept constant at 40 m^3/s through all simulations, and so was the production rate of cement and inlet bed material temperature coming from the calciner, which were set to 227 ton/h and 900°C respectively. In Table 3.1 dimensions and process conditions used for modelling the reference case can be seen. These values are based on the process conditions at Cementa. Additionally, based on the possibility to impact the heat transfer to the bed material, several parameters were modelled with varied values. However, for the reference case the values of these varying parameters were set to be based on the process at Cementa. The bed volume portion seen in Table 3.1 is the percentage of the kiln volume filled with solid bed material, which was set to approximately 10% for the reference case. To simulate this in the model, approximately 10% of the cells of the kiln was set as bed material at the bottom of the kiln. The amount of bed material present in the kiln changes the required heat to reach a desired outlet temperature of the bed material. As mentioned in section 2.2, the kiln rotates to mix and simultaneously move the bed material downstream, the rotational speed of the kiln was set to 3.8 rpm for the reference case. Furthermore, the inlet and outlet gas temperatures of the gas stream called secondary air in Figure 3.1, were set to 980°C and 1200°C respectively for the reference case. Lastly, the emissivity has been set to 0.8 for both the bed and walls, these are however rather uncertain values based on literature and estimations, therefore the effect the emissivity has on the results was investigated in a sensitivity analysis.
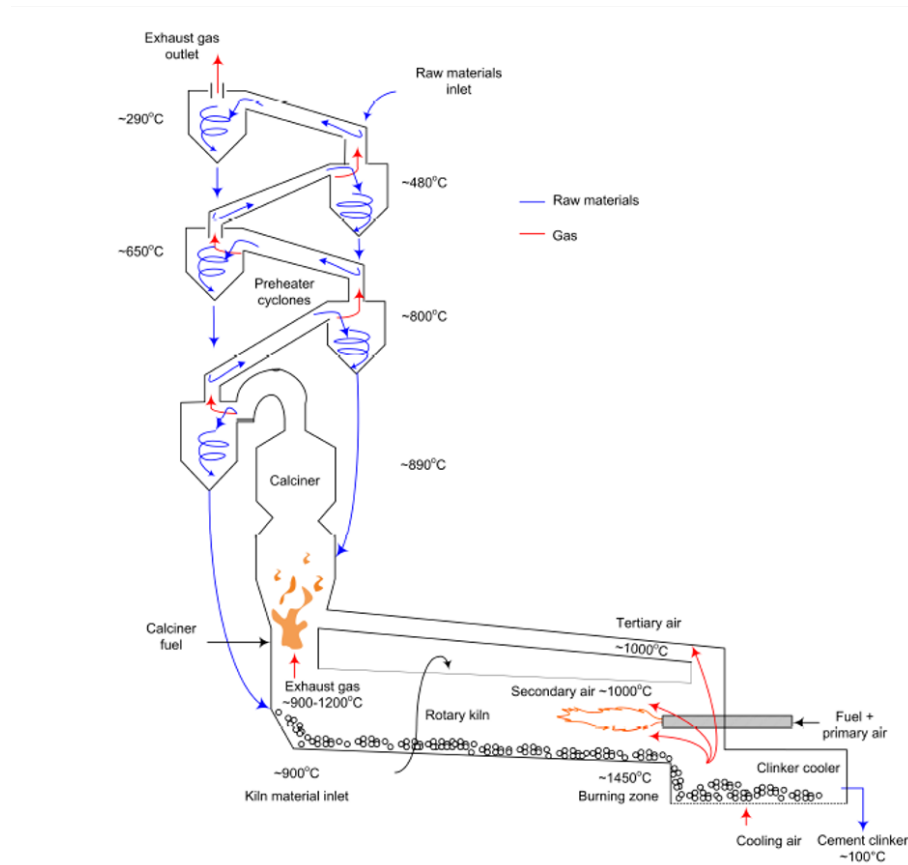
Figure 3.1: Schematic of the cyclone tower with calciner, rotary kiln and cooler. Raw material flow and gas flow indicated by blue and red arrows respectively. Courtesy to Cementa for providing the figure

Table 3.1: Approximate dimensions and process conditions for modeling the reference coal and plasma case.

Parameter	Value
Kiln radius	2.1 m
Kiln length	80 m
Bed volume portion	10%
Production rate	227 ton/h
Rotational speed of kiln	3.8 rpm
Gas inlet temperature	980°C
Gas outlet temperature	1200°C
Bed inlet temperature	900°C
Gas flow rate	40 m^3/s
Emissivity	0.8

Firstly, the reference coal case was modelled in order to compare the results with the plasma case, as well as in order to validate the model against measured values of the outer wall surface temperature provided from the kiln at Slite. Thereafter, different simulation cases were run with a plasma as heat source. The parameter values

that differ between the simulations with a coal flame and a plasma, except for gas compositions and temperature profiles etc, are listed in Table 3.2. The parameter "projected surface area of particles" is the surface area of the particles per kilogram present within the kiln, which for the coal case was set to 153.61 m²/kg. For the plasma reference case, which contained the first set of parameter values to model, the projected surface area of particles has been set to 0 m²/kg, since there are naturally no particles present in the kiln when no solid fuels are combusted. In the modelling tool the axial data input points for both the coal and plasma cases were set at 10, 30, 50 and 70 meters away from the burner. The particle concentration profile was set so that the particle surface area was reduced moving away from the burner. At 10 meters from the burner it was set so that a 100% of the projected surface area was remaining, at 30 meters the surface area was reduced to 90% of the original value, at 50 meters it was 67% and at 70 meters it was set to 13.5% of the original value. The highest burner temperature, is set to 2000°C for the coal flame, with temperature profiles based on experimental values from a pilot scale kiln for iron ore, and from Cementas experience. Details about the measurements and the pilot kiln can be seen in the paper by Gunnarsson et al.[19]. The temperature profile for the coal case can be seen in Table 3.3. The highest temperature of the plasma has been set to 2500°C for the reference case, where the temperature profile has been based on estimated values, which can be seen in Table 3.4. In the modelling tool, the temperature profiles were specified by setting temperatures at different positions in the axial and radial directions. Lastly, the gas concentration profiles for the plasma case were set so that the gas contained a 100% carbon dioxide throughout the entire kiln. For the coal case, the gas concentration profile used can be seen in Table 3.5. In Tables 3.3 to 3.5, the axial positions are 10, 30 and 50 meters from the burner respectively, referred to as axial positions 1, 2 and 3 in the tables, and the radial positions are distributed from the center of the kiln towards the wall in radial direction, thus, radial position 1 is closest to the center and radial position 5 is closest to the wall.

Table 3.2: Reference case parameter values for coal & plasma

Parameter	Coal value	Plasma value
Projected surface area of particles	153.61 $\frac{m^2}{kg}$	0
Highest burner temperature	2000°C	2500°C

Table 3.3: Temperature profile for the coal case. Temperature given at each axial and radial position.

	rad pos 1	rad pos 2	rad pos 3	rad pos 4	rad pos 5
T (°C), axial position 1	1888	1708	1366	1338	1333
T (°C), axial position 2	1823	1709	1445	1430	1394
T (°C), axial position 3	1675	1638	1539	1517	1494

Table 3.4: Temperature profile for the plasma reference case. Temperature given at each axial and radial position.

	rad pos 1	rad pos 2	rad pos 3	rad pos 4	rad pos 5
T (°C), axial position 1	1966	1779	1423	1394	1389
T (°C), axial position 2	1899	1780	1506	1490	1453
T (°C), axial position 3	1745	1706	1603	1580	1556

Table 3.5: Gas concentration profile for the coal case. Gas portion of H_2O and CO_2 shown in % at each axial and radial position.

	rad pos 1	rad pos 2	rad pos 3	rad pos 4	rad pos 5
H_2O (%), position 1	4.41	3.17	0.79	0.76	0.77
H_2O (%), position 2	4.15	3.48	1.19	1.08	0.82
H_2O (%), position 3	2.93	2.71	1.59	1.70	0.97
CO_2 (%), position 1	6.89	4.97	1.23	1.19	1.20
CO_2 (%), position 2	5.57	4.68	1.60	1.46	1.11
CO_2 (%), position 3	4.97	4.61	2.70	2.89	1.64

3.1.1 Plasma simulation cases

The plasma differs from the coal case by the absence of particles, which affects the radiation. Furthermore, the radiation properties are different due to a changed gas composition and increased temperatures.

Table 3.6 show how the previously mentioned parameters for the reference case has been varied, within a certain range, to examine the effects on the heat transfer mechanisms. Starting from the top of the table, the gas inlet temperature to the kiln was varied between 980°C and 2500°C. Since the gas coming out of the cooler and in to the kiln is 980°C to begin with, it would be needed to preheat the gas before the kiln. To supply the heat needed, an extra plasma torch for example could be installed. Because of the cooler after the kiln, the lower temperature in the selected range is set to 980°C in order to not affect the performance of the cooler. The upper value is an estimation of a perhaps unreasonable temperature, simply to see the effects it has on the heat transfer mechanisms. The temperatures in the case with a varying burner temperature is the highest temperature of the plasma, at the position at the center in radial direction and close to the burner. By varying the highest temperature close to the burner, the entire temperature profile also needs to be adjusted. In the model, the temperatures set at different positions in the kiln, building up the temperature profile, were set as a percentage of the highest temperature, with a fading effect in radial and axial directions. That is, when the highest temperature close to the burner is increased, all the other temperatures in the temperature profile are also increased, while simultaneously keeping the same relation between them. When the values of the temperature profile for the burner is increased, the heat transfer to the bed material should also increase, due to the larger temperature gradient. Particles present in the kiln help spread radiation, which is desirable, through scattering. Therefore, the addition of particles, which

otherwise are absent in the plasma case, was examined. The amount of particles given in Table 3.6 is the percentage of the projected surface area of the particles contained in the coal case. The projected surface area of particles seen in Table 3.2 for the coal case was hence, simply multiplied by a portion, ranging from 0 to 0.15, in the model setup to simulate the addition of particles. In reality, the particles, in form of char, would have to be added to the kiln. The effects the rotational speed would have on the heat transfer was also examined, since it is an easily controllable parameter which could potentially improve or worsen the heat transfer. The rotational speed was both increased and decreased from the reference case, with speeds ranging from 2 to 4.2 rpm. The bed portion with values given in volume percent of the kiln, occupied by solid material, was varied from 5 to 14 % to examine a reduction and an increase compared to the reference case. Lastly, the effect the bed and inner wall emissivity had on the results was studied separately, since these values were considered uncertain, and thus the impact of the uncertainty had to be examined. A change in emissivity should affect the amount of radiation emitted, but also absorbed, from a source, since it is defined as the ratio between the actual radiation emitted from a surface compared to that emitted from a perfect emitter.

Table 3.6: Different cases modelled with a plasma

Case/Parameter	Range and unit
Gas inlet temp	980-2500°C
Burner temp	1900-2800°C
Particle amount	0-15 %
Rotational speed	2-4.2 rpm
Bed portion	5-14 %
Inner wall emissivity	0.4-1
Bed emissivity	0.1-1

3.2 Energy balances

The following balances are used to calculate the amount of heat required in each part of the kiln. Equation 3.1 describes how the energy supplied to the burner, in form of fuel, is further distributed in the kiln in form of energy for reactions, heat to the bed and gas as well as heat losses. The energy transferred to the gas and bed can be seen in equations 3.2 and 3.3 respectively, where the transferred energy is equal to the difference between the enthalpy at the outlet and the inlet. The expression for the enthalpy difference is then further elaborated by the mass, specific heat and temperature difference. The energy losses, in form of heat lost by convection and radiation is expressed in equation 3.4, where the expressions for the convection and radiation losses, from medium i to j, are described in equations 3.5 and 3.6 respectively. Furthermore, the energy required for the reactions, expressed in equation 3.7, is calculated by the sum of the temperature difference multiplied with the mass and heat of formation for each species.

$$Q_{burner} = Q_{reaction} + Q_{bed} + Q_{gas} + Q_{losses} \tag{3.1}$$

$$Q_{gas} = H_{gas,out} - H_{gas,in} = (\dot{m}CpT)_{gas,out} - (\dot{m}CpT)_{gas,in} \tag{3.2}$$

$$Q_{bed} = H_{bed,out} - H_{bed,in} = (\dot{m}CpT)_{bed,out} - (\dot{m}CpT)_{bed,in} \tag{3.3}$$

$$Q_{losses} = Q_{convection,losses} + Q_{radiation,losses} \tag{3.4}$$

$$Q_{convection,losses} = UA\Delta T \tag{3.5}$$

$$Q_{radiation,losses} = \epsilon\sigma(T_i^4 - T_j^4)A \tag{3.6}$$

$$Q_{reaction} = \sum_i (m_i T_{out} - m_i T_{in})h_{f,i} \tag{3.7}$$

In equations 3.1 to 3.7, Q is the required heat for each of the indices seen in the equations. $\dot{m}$ is the mass flow, Cp is the specific heat capacity, T is temperature, H is the enthalpy, ϵ is the emissivity coefficient, σ is the Stefan-Boltzmann constant, A is the area, U is the overall heat transfer coefficient and h_f is the heat of formation which has been gathered from the software FactSage for a certain composition of raw meal. The modelling tool calculates for example outlet bed temperatures and wall temperatures, these temperatures can then be used to check if equation 3.1 adds up. If not, the temperature of the outlet gas for instance needs to be adjusted. The calculated Q's from equation 3.1 to 3.7 are later used to analyze the results from the simulated cases.

3.3 The iteration process in Matlab

As previously mentioned, the simulations have been performed in a modelling tool in Matlab, which has been previously developed at Chalmers. The solving scheme of the model begins with dividing the volume of the kiln into a set number of cells, where more cells means longer computational times but more accurate solutions. First, the iteration process solves for the intensities from the RTE equation in all cells. Thereafter, the heat flux to the bed and wall surfaces are determined, where the temperatures are calculated from the convective, conductive and radiative heat transfer equations. All cells are then moved one step in the same direction as the kiln, to simulate its rotation, and the calculation is repeated for new heat fluxes and temperatures, until the temperature has converged. The iteration steps, from solving for the intensities from the RTE, are then repeated until the entire system has converged, and the solution has, thus, been obtained.

3.4   Model development

The absorption coefficients in the equations for radiation remained constant during the early simulations, due to the assumption of a carbon dioxide concentration of 100% and no dissociation occurring in the plasma. Since the absorption coefficients are dependent on the gas composition, they remained constant. Furthermore, the absorption coefficients are connected to a parameter in the model which is weighted against certain wavelengths. The expression that was used early in the project for handling the weighting did not work for the high temperatures occurring in a plasma, a new expression was therefore implemented with new parameters to resolve this issue.

4

Results & discussion

The results from the simulated cases will be presented in this section beginning with the coal flame simulation and validation of the model, followed by various simulations with a plasma. Lastly, the results from the sensitivity analysis is presented.

4.1 Coal flame simulation

First a simulation of a coal flame was made, in order to see that the model was working as intended, that the results were comparable to reality, and to be able to compare the coal flame with the plasma. As mentioned in the method chapter, the temperature profile of the coal flame is partly based on experiments made on a pilot scale kiln for iron ore pellets and partly based on observations from Cementa. In Figure 4.1, we can see the axial temperature profile of the coal flame. It can be observed from this figure that the flame keeps a relatively high temperature quite far into the kiln, looking at the x-axis, 50 meter away from the burner, the temperature is still around 2000 K while close to the burner the temperature is just below 2300 K, this is due to that a long flame was assumed for the coal case. This temperature profile is typical for a coal flame, in later sections we can compare this profile to the predicted temperature profile from a plasma burner.
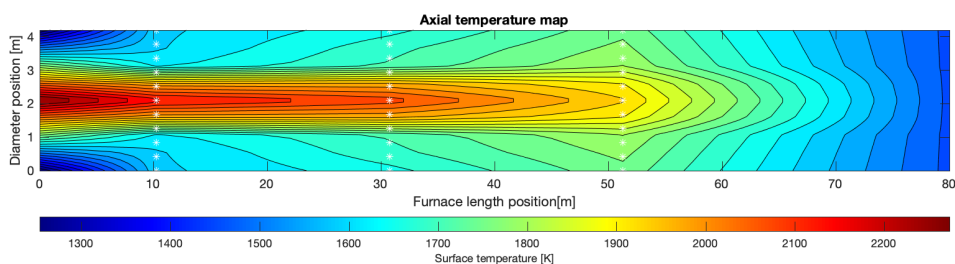
Figure 4.1: Axial temperature map of a coal flame in the rotary kiln, on the x-axis the length of the kiln is shown and on the y-axis the diameter of the kiln can be seen. The temperature is shown with different colors displayed beneath the temperature map.

Having the temperature profile for the flame seen in Figure 4.1 gives a temperature map of the kiln walls and bed seen in Figure 4.2. The "lower" section in Figure 4.2 is the bed material, having slightly lower temperature than the walls throughout the kiln. Studying the bed temperature at the end of the kiln, at length position 0, it

can be observed that the bed reaches a temperature slightly above 1450°C, which is the desired temperature of the bed at the outlet of the kiln. A relatively smooth temperature profile can also be noted along the kiln length, which is desirable in order to give sufficient time for the reactions to occur. The simulation was performed with 8 discrete ordinates, 20 cells in the radial direction, 40 cells in the axial direction and 48 cells in the angular direction.
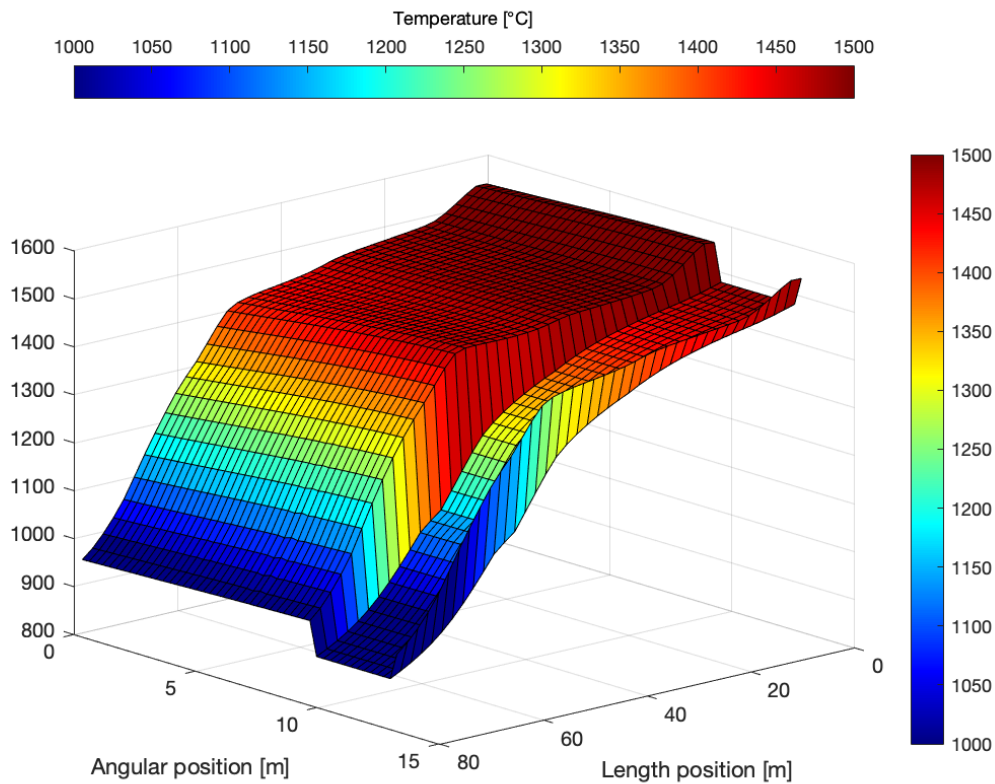
Figure 4.2: Three dimensional temperature map of the kiln walls and bed for the coal case. Temperature on one axis (also shown in colors), angular position in meters displayed on the second axis, and the length position in meters on the last axis.

The total heat demand and the amount of heat transferred by the different heat mechanisms etc for this case can be seen in the Table 4.1.

Table 4.1: The amount of heat from radiation, convection and conduction to bed as well as heat losses, heat to gas and bed temperature at outlet for the coal case.

Radiation to bed	26.16 MW
Convection to bed	2.59 MW
Conduction to bed	22.99 MW
Total heat to bed	51.74 MW
Outer heat losses	1.78 MW
Total heat to gas	12.01 MW
Energy balance error	0.41 MW
Total heat demand	65.53 MW
Bed temperature at outlet	~ 1453°C

It can be noted from Table 4.1 that the majority of heat received by the bed comes from radiation, followed by conduction and lastly a small amount from convection through the gas. According to these results seen in the table, the total heat demand for this case, with a coal flame, is 65.53 MW to reach a bed outlet temperature of approximately 1450°C.

4.1.1 Validation of coal model

The simulation of the coal flame was compared to measured data from the actual kiln at Slite to see how well the model predicts reality. Measurements are, as mentioned before, difficult to execute within the kiln, however, measurements on the outside wall has been made with an IR-camera, which can be seen in Figure 4.3 below compared to the values from the model.
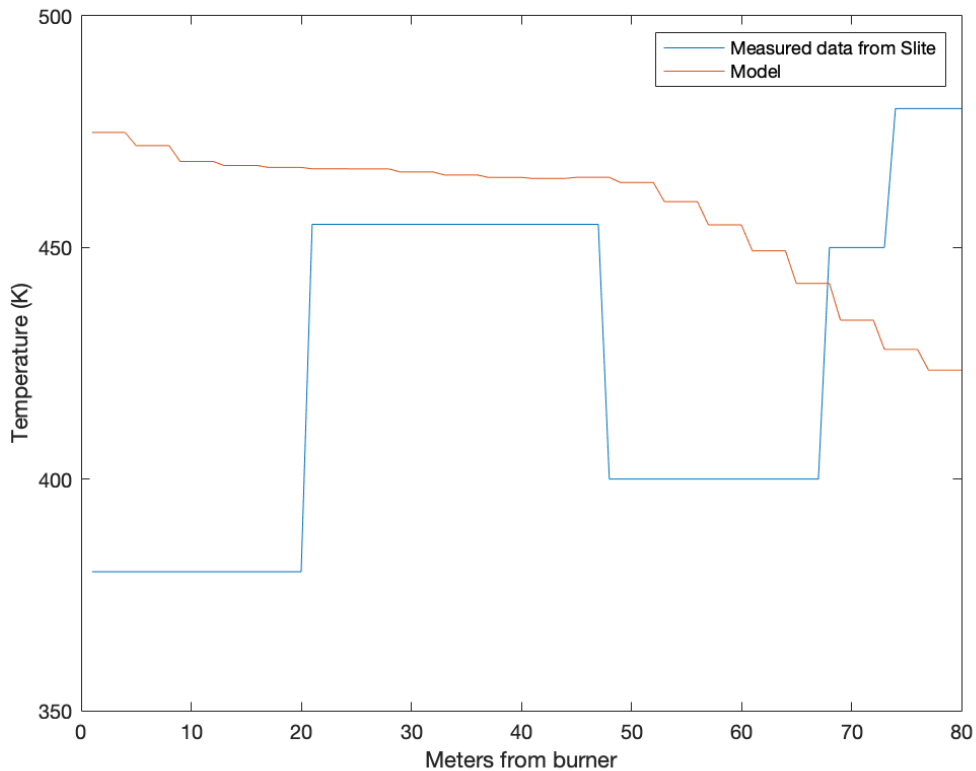
Figure 4.3: Measured and model values of outer wall temperature of the rotary kiln with a coal flame

The values obtained from the model seem to match the measured values from the kiln at Slite fairly well, according to Figure 4.3, especially in the middle section of the kiln. The deviation could be caused by the build up of material in different parts of the kiln, creating thicker walls in certain places, which prevents the transport of heat to the outside surface of the kiln walls. In the model the bed simply passes through the kiln, without considering any build up. Furthermore, the validation was made to see if the set values for the thermal conductivity needed adjustment, which was concluded not to be necessary.

4.2   Plasma simulation

The plasma was simulated with similar process conditions and dimensions as the coal flame. However, for the plasma case, the gas composition, the temperature profile, the absence of particles and the radiative properties are different. The reference case parameter values can be seen in Table 3.2 in the method section and the results from the simulations of this case will be presented first. A three dimensional temperature map for the plasma reference case can be seen in Figure 4.4.
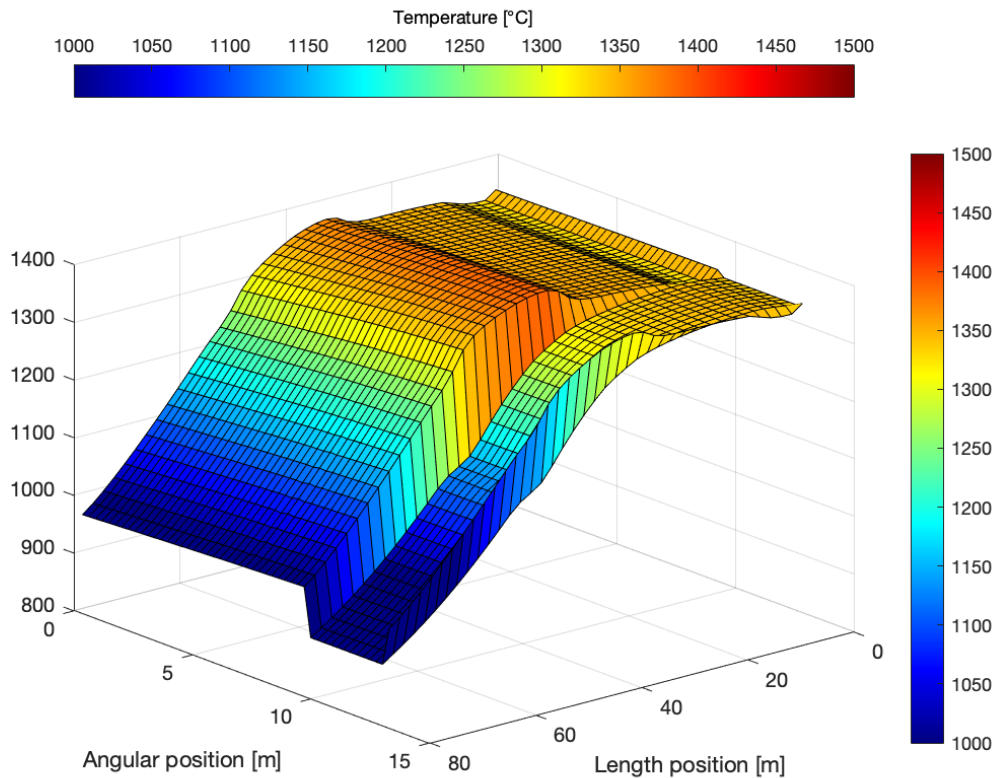
Figure 4.4: Three dimensional temperature map of the kiln walls and bed for the plasma base case. Temperature on one axis (also shown in colors), angular position in meters displayed on the second axis, and the length position in meters on the last axis.

Table 4.2 presents the energy balance for the plasma reference case. As may be observed in the table, there seems to be equal contributions of heat transferred to the bed from radiation and conduction while the convection appear to contribute less.

Table 4.2: The amount of heat from radiation, convection and conduction to bed as well as heat losses, heat to gas and bed temperature at outlet for the plasma base case.

Radiation to bed	14.62 MW
Convection to bed	6.68 MW
Conduction to bed	14.38 MW
Total heat to bed	35.69 MW
Outer heat losses	1.63 MW
Total heat to gas	22.90 MW
Energy balance error	0.36 MW
Total heat demand	60.22 MW
Bed temperature at outlet	1336°C

Note that the outlet bed temperature, which can be seen in Figure 4.4 and in Table 4.2, does not reach a temperature of 1450°C. Different methods and the impact of different parameters on the outlet temperature, among others, were thus investigated in the following cases simulated.

4.2.1 Difference between plasma and coal temperature profile

As mentioned previously in the theory section, a plasma produces a much more concentrated temperature profile than the temperature profile from a coal flame. The difference between the two can be seen in Figure 4.5, where the temperature profile for the plasma is seen at the top and the temperature profile of the coal flame can be seen at the bottom. From observing the figure, it can be noted that the temperature at the center of the plasma, at position 0 meters into the kiln and at the centre diameter position, is much higher than the temperature at the same position for the coal case. Furthermore, the temperature is thought to fade quickly for the plasma as we move from length position 0 towards the other end of the kiln, while the coal case keeps its temperature much further into the kiln. This is mainly due to the absence of particles in the plasma case, which lowers the heat transfer since there are no particles that scatter radiation.
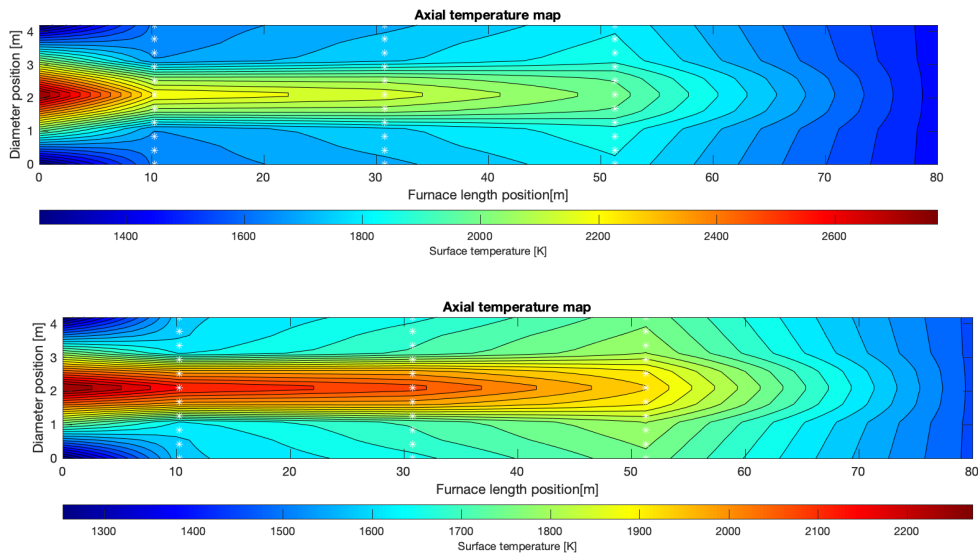
Figure 4.5: Axial temperature map of the reference case for plasma at the top and reference case for coal at the bottom. Furnace length position along the x-axis, diameter position along the y-axis and the temperature indicated by colors

Due to the increased temperatures in the plasma compared to the coal flame, dissociation of the carbon dioxide molecules could potentially affect the results. Currently, the dissociation has not been included in the model, therefore, the impact from the dissociation should be further examined to ensure reliable results.

4.2.2   Varying plasma temperature

By varying the temperature of the plasma, the temperature difference between the plasma and the bed is either increased or decreased compared to the reference case. If the temperature difference is increased, the outlet bed temperature should increase as well, which can be seen in Table 4.3. The burner temperature in the table is the temperature at the center of the plasma. From the implementation of the temperature profile, it follows that the total temperature profile is increased for the plasma as the burner temperature is increased. Note that the desired outlet bed temperature of 1450°C is achieved at a temperature just below 2750°C for the burner temperature. Furthermore, at these temperatures, the majority of the heat transferred to the bed comes from radiation followed by conduction as can be seen in the table. The reason for the high heat transfer from conduction could be because of high radiation to the walls, which increases their temperature and further transfers heat through conduction to the bed. Also, it can be noted that the total heat demand when the outlet bed temperature reaches 1450°C (at burner temp 2750°C) is higher than the case with a coal flame, which can be seen in Table 4.1. This is partly because of the higher heat transfer to the gas, due to a higher specific heat capacity of carbon dioxide compared to the specific heat capacity of air, which is the gas in the coal case. However, the inlet and outlet gas temperatures remained the same for the plasma case and the coal case. Additionally, rather odd results were obtained at a burner temperature of 2200°C, which can be seen on the energy balance error and that the temperature of the bed at the outlet has not changed when the burner temperature was increased. This can be seen as an outlier and does not affect the conclusions that can be drawn from these results but should be further examined to rule out errors in the model or in the implementation of the input data.

Table 4.3: Outlet bed temperature, heat transfer mechanisms to the bed, heat losses and heat demand for varying burner temperatures

Burner temp (°C)	1900	2000	2200	2300	2400	2500	2600	2700	2725	2750	2800
Outlet bed temp (°C)	1092	1116	1116	1244	1278	1336	1385	1428	1440	1452	1475
Radiation (MW)	5.54	7.02	12.24	10.82	12.86	14.62	16.97	19.45	20.08	20.72	22.11
Convection (MW)	3.01	3.79	6.44	5.75	6.32	6.68	7.19	7.65	7.75	7.86	8.08
Conduction (MW)	6.12	7.70	13.22	11.47	13.14	14.38	16.00	17.59	17.97	18.35	19.15
Total heat to bed (MW)	14.68	18.51	31.90	28.04	32.33	35.69	40.16	44.68	45.81	46.93	49.34
Outer heat losses (MW)	1.37	1.41	1.45	1.53	1.58	1.63	1.68	1.73	1.74	1.76	1.78
Heat to gas (MW)	22.90	22.90	22.90	22.90	22.90	22.90	22.90	22.90	22.90	22.90	22.90
Energy balance error (MW)	-0.02	2.82	16.21	0.62	2.46	0.36	-0.83	0.42	0.36	0.35	0.49
Total heat demand (MW)	38.95	42.82	56.26	52.47	56.81	60.22	64.74	69.31	70.45	71.59	74.03

The temperature map for the case which reaches an outlet bed temperature of 1450°C can be seen in Figure 4.6. Similarly as the coal case, the temperature profile of the bed seen in Figure 4.6 is quite smooth.
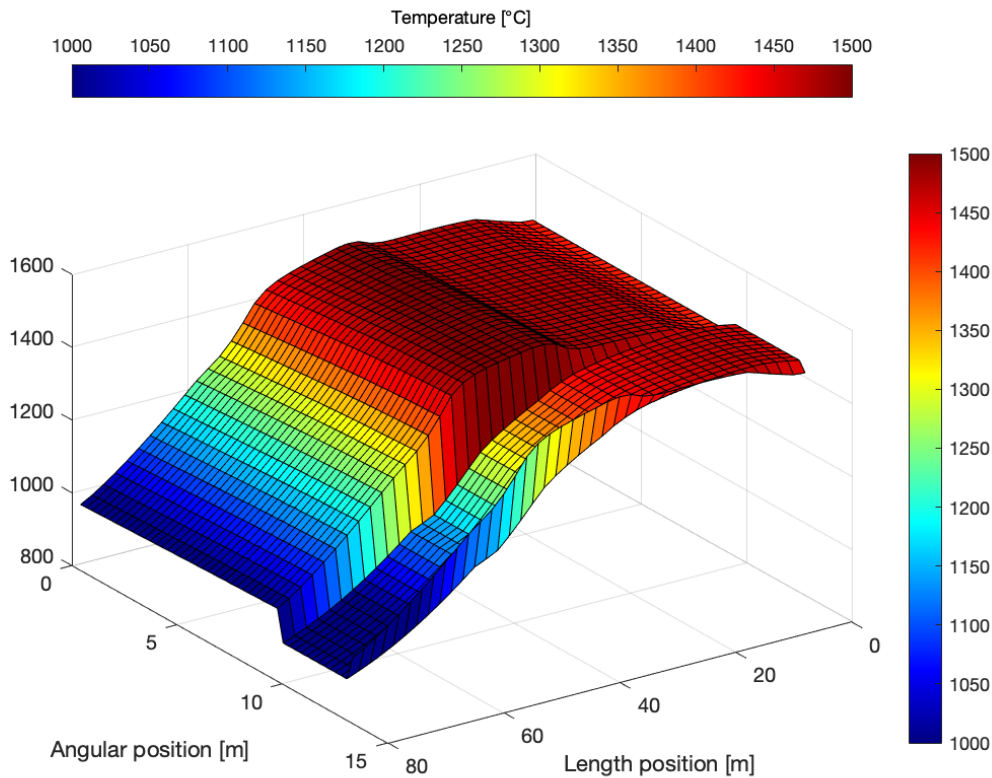
Figure 4.6: Three dimensional temperature map of the kiln walls and bed for a plasma case with a maximum burner temperature of 2750°C. Temperature on one axis (also shown in colors), angular position in meters displayed on the second axis, and the length position in meters on the last axis.

4.2.3 Varying particle content

When introducing particles in the kiln, heat transfer from radiation is increased, which can be seen in Figure 4.4. In the table the percentage (%) is related to the amount of particles present in the kiln for the reference coal case, where the particles projected surface area has been set to 153.61 m^2/kg. From Table 4.4 it can be seen that the outlet bed temperature reaches the desired value of 1450°C when the kiln contains an amount of particles corresponding to 9% of the projected surface area of the particles present during coal combustion. As mentioned previously, the high contribution from conduction is likely due to heat being radiated to the walls from the plasma, which in turn transfers heat to the bed through conduction. Also, in Figure 4.7 it can be seen that the surface temperature of the walls increase as the amount of particles are increased, which also supports the previous argument of why the conduction is increased. Furthermore, heat to gas is constant as the particles are increased due to that inlet and outlet gas temperatures are kept constant, so a higher particle content only results in a higher velocity of the gas passing through the kiln.

Table 4.4: Outlet bed temperature, heat transfer mechanisms to the bed, heat losses and heat demand for varying particle content compared to particle content present in coal flame

% particles	0	1	2	3	4	5	6	7	8	9	10	15
Outlet bed temp (°C)	1336		1369	1383	1393	1401	1411	1433	1442	1450	1459	1488
Radiation (MW)	14.62	15.88	17.00	18.03	18.99	19.94	20.81	21.33	21.98	22.57	23.15	25.40
Convection (MW)	6.68	6.46	6.26	6.08	5.91	5.77	5.65	5.43	5.30	5.17	5.05	4.57
Conduction (MW)	14.38	15.41	16.30	17.10	17.83	18.54	19.19	19.53	19.99	20.40	20.79	22.29
Total heat to bed (MW)	35.69	37.76	39.55	41.20	42.73	44.25	45.65	46.29	47.27	48.14	48.99	52.27
Outer heat losses (MW)	1.63	1.64	1.66	1.67	1.68	1.69	1.70	1.71	1.72	1.73	1.73	1.76
Heat to gas (MW)	22.90	22.90	22.90	22.90	22.90	22.90	22.90	22.90	22.90	22.90	22.90	22.90
Energy balance error (MW)	0.36	0.31	0.26	0.18	1.12	1.55	2.06	0.54	0.51	0.45	0.44	0.43
Total heat demand (MW)	60.22	62.30	64.11	65.77	67.32	68.85	70.25	70.90	71.89	72.77	73.62	76.93
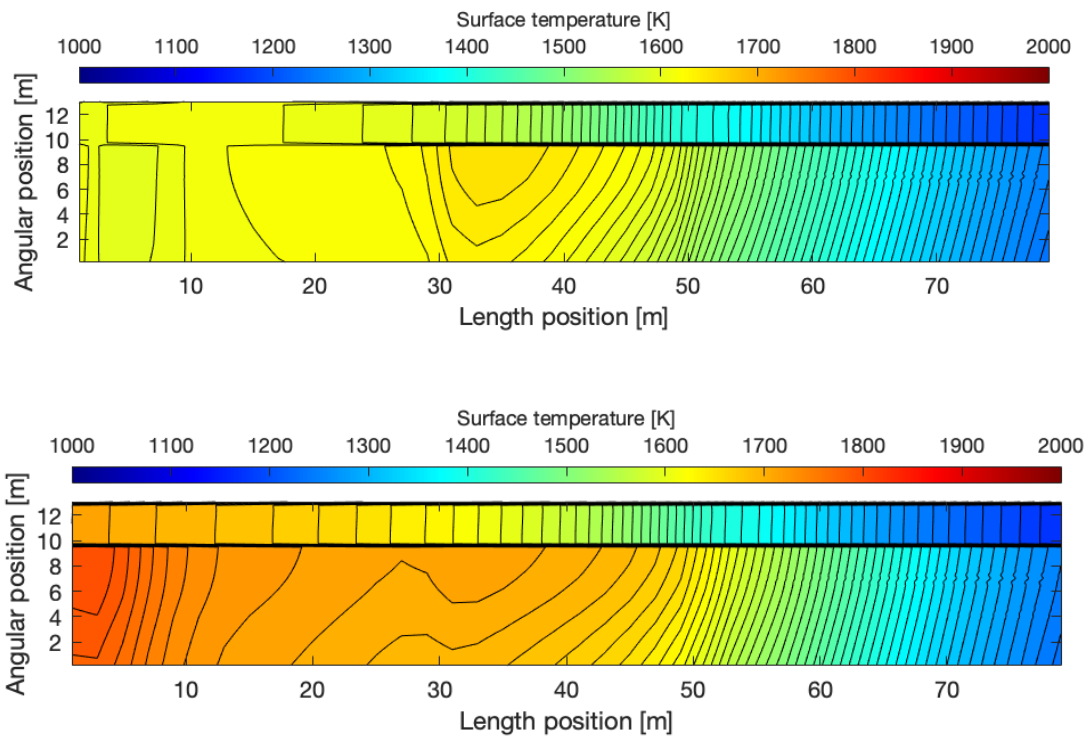
Figure 4.7: Surface temperature of the kiln walls, 0% particles on the top and 9% particles on the bottom. Percentage indicates the particle surface area compared to particles in the coal case. Length position of the kiln along the x-axis and angular position along the y-axis. Temperature is indicated with colors.

The temperature map of the bed and walls can be seen in Figure 4.8 for the case with 9% particles. It can be noted that the temperature profile is smooth throughout the length of the kiln.
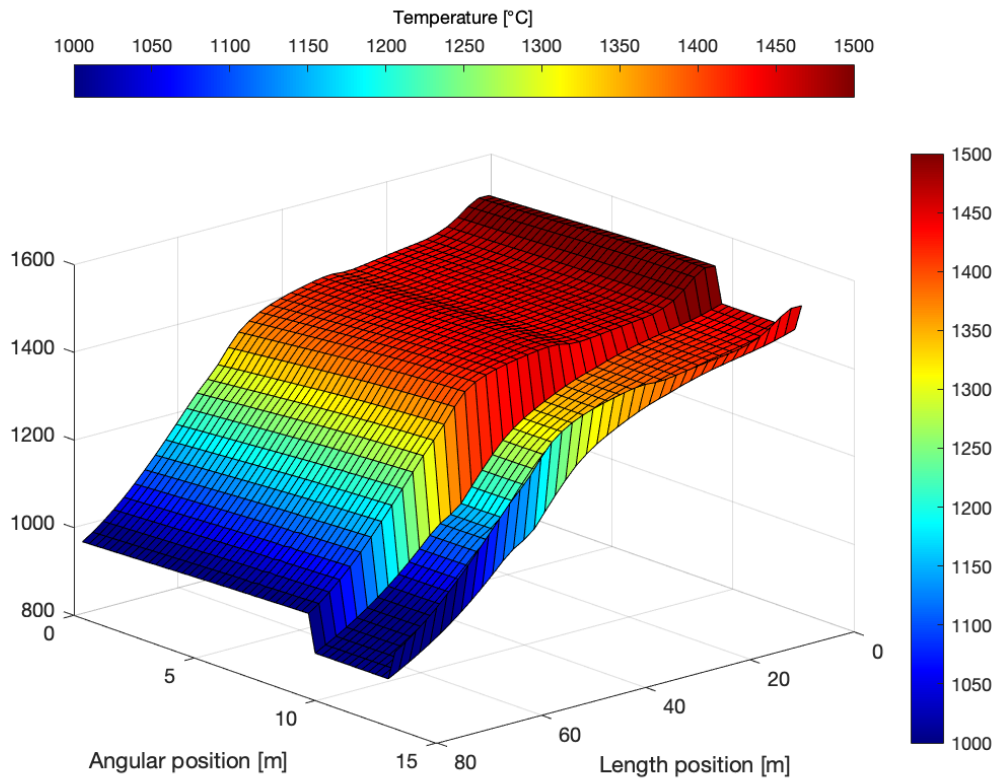
Figure 4.8: Three dimensional temperature map of the kiln walls and bed for a plasma case with an added particle content of 9% of the particles present in a coal fired system. Temperature on one axis (also shown in colors), angular position in meters displayed on the second axis, and the length position in meters on the last axis.

4.2.4 Varying inlet gas temperature

Preheating the gas that enters the kiln at the burner end causes the passing gas to transfer heat to the bed instead of receiving heat from the kiln. In Table 4.5 it is shown that the outlet bed temperature increases as the inlet gas temperature is increased, which is expected. However, the outlet bed temperature does not reach the required 1450°C even though the inlet gas temperature is heated up to 2500°C. This is due to the assumption that only the inlet gas temperature changes and not the entire gas temperature profile, hence, the inlet gas temperature only affects the heat transfer before the first axial position where data is entered, which is 10 meters from the burner. The inlet gas could be further increased until a satisfactory outlet bed temperature, however heating the gas to that degree is probably not reasonable or efficient. From Table 4.5, note that heat to gas is 0 at an inlet gas temperature of 1200°C since both the inlet and outlet gas temperature is 1200°C. At higher temperatures than 1200°C the heat to gas becomes negative since the inlet temperature is higher than the outlet gas temperature which is constant at 1200°C. The total heat demand also becomes negative for high inlet gas temperatures, however, the

gas needs to be heated before entering the kiln, which requires energy.

Table 4.5: Outlet bed temperature, heat transfer mechanisms to the bed, heat losses and heat demand for varying inlet gas temperatures

Inlet gas temp (°C)	980	1200	1400	1600	1900	2000	2200	2400	2500
Outlet bed temp (°C)	1343	1350	1358	1366	1379	1384	1398	1411	1417
Radiation (MW)	14.46	15.21	16.04	16.95	18.54	19.12	20.41	21.72	22.38
Convection (MW)	6.72	7.26	7.75	8.22	8.93	9.17	9.64	10.10	10.33
Conduction (MW)	14.57	15.17	15.81	16.47	17.53	17.90	18.68	19.41	19.76
Total heat to bed (MW)	35.75	37.64	39.59	41.65	45.00	46.19	48.73	51.24	52.47
Outer heat losses (MW)	1.63	1.63	1.64	1.64	1.65	1.66	1.66	1.67	1.67
Heat to gas (MW)	22.90	0	-21.26	-42.83	-75.63	-86.66			
Energy balance error (MW)	0.16	0.19	0.23	0.14	0.16	0.15	0.22	0.23	0.28
Total heat demand (MW)	60.29	39.27	19.98	0.46	-28.98	-38.82			

A three dimensional temperature map of the kiln walls and bed can be seen in Figure 4.9, for an inlet gas temperature of 2000°C. Comparing this temperature map with earlier results, the temperature profile for the walls is relatively steep towards the end of the kiln, since the temperature gradient between the inlet gas and the bed material at the end of the kiln becomes large when the inlet gas temperature is increased.
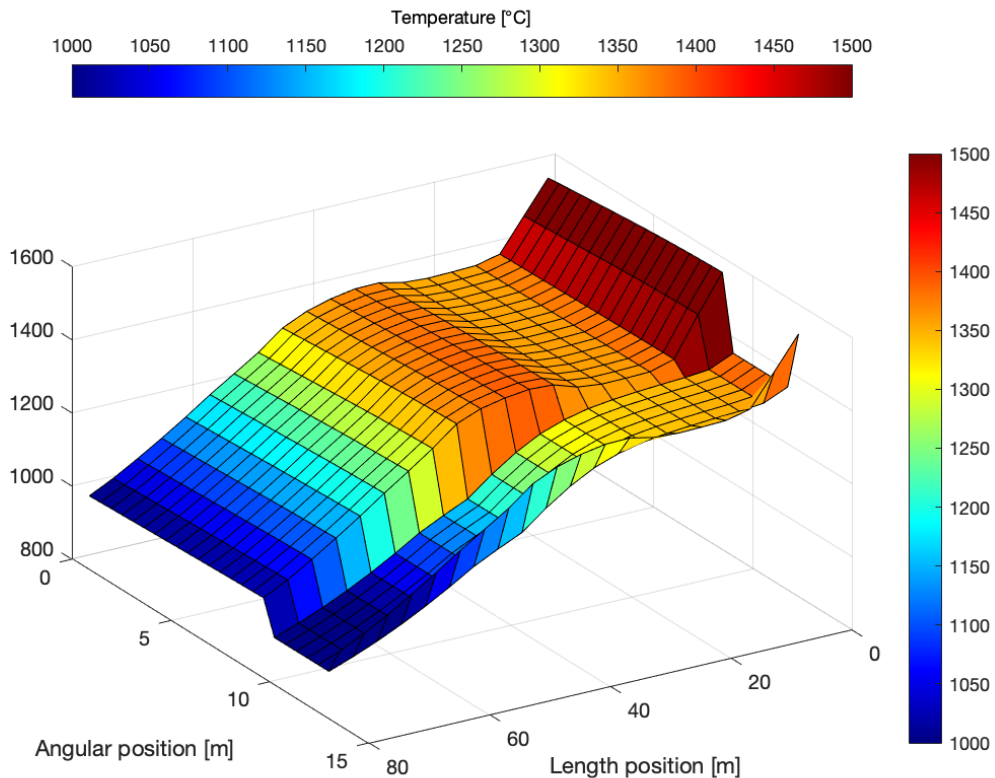
Figure 4.9: Three dimensional temperature map of the kiln walls and bed for a plasma case with an inlet gas temperature of 2000°C. Temperature on one axis (also shown in colors), angular position in meters displayed on the second axis, and the length position in meters on the last axis.

4. Results & discussion

4.2.5   Varying rotational speed

Since the rotational speed of kiln can easily be controlled, it is a parameter that investigated how it affects the heat transfer to the bed to see if it can be easily increased. The results from varying the rotational speed can be seen in Table 4.6. From the table it can be noted that the outlet bed temperature barely changes as the rotational speed is increased or decreased from the standard value of 3.8 rpm. However, note that at rotational speed 4.2 rpm the total heat to bed is increased from lower rpm but the outlet bed temperature is lower, which is contradicting. Note also that the energy balance error for this case is significantly larger than for the other rotational speeds. The results for 4.2 rpm does thus not seem very accurate.

Table 4.6: Outlet bed temperature, heat transfer mechanisms to the bed, heat losses and heat demand for varying kiln rotational speeds

Rotational speed (rpm)	2	2.2	2.4	2.6	2.8	3	3.2	3.4	3.8	4.2
Outlet bed temp (°C)	1337	1337	1340	1339	1340	1340	1351	1345	1343	1312
Radiation (MW)	15.70	15.54	15.20	15.21	15.08	14.96	13.89	14.41	14.46	15.14
Convection (MW)	6.98	6.95	6.84	6.89	6.86	6.84	6.36	6.64	6.72	7.05
Conduction (MW)	12.50	12.83	12.94	13.37	13.62	13.86	13.05	13.91	14.57	15.70
Total heat to bed (MW)	35.19	35.32	34.98	35.46	35.57	35.67	33.30	34.95	35.75	37.88
Outer heat losses (MW)	1.63	1.63	1.63	1.63	1.63	1.63	1.64	1.63	1.63	1.62
Heat to gas (MW)	22.90	22.90	22.90	22.90	22.90	22.90	22.90	22.90	22.90	22.90
Energy balance error (MW)	0.06	0.05	0.04	0.06	0.05	0.06	0.05	0.09	0.16	5.20
Total heat demand (MW)	59.72	59.85	59.52	60.00	60.10	60.20	57.85	59.49	60.29	62.41

4.2.6   Varying bed portion

Similarly to varying the rotational speed of the kiln, the bed portion can also be increased or decreased easily to potentially control or impact the heat transfer to the bed. The results shown in Table 4.7 shows that a large volume portion of the bed decreases the outlet bed temperature, which is logical since there is more bed material to heat up. Furthermore, both radiation and convection increases as the bed portion increases. This could be due to that there is an increased surface area at the top of the bed which is exposed to the flame and gas. The conduction however decreases slightly which could potentially be explained by that there is less wall above the the bed as the bed portion increases, the walls thus become colder and the heat transfer through conduction is thus reduced.

Table 4.7: Outlet bed temperature, heat transfer mechanisms to the bed, heat losses and heat demand for varying bed portions

Bed portion	0.0546	0.0908	0.1379
Outlet bed temp (°C)	1344	1338	1309
Radiation (MW)	14.06	14.76	15.48
Convection (MW)	5.47	6.64	8.13
Conduction (MW)	14.89	14.48	14.35
Total heat to bed (MW)	34.42	35.89	37.96
Outer heat losses (MW)	1.37	1.63	1.88
Heat to gas (MW)	22.90	22.90	22.90
Energy balance error (MW)	0.18	0.33	5.68
Total heat demand (MW)	58.70	60.43	62.74

4.3 Sensitivity analysis

The bed emissivity and inner wall emissivity are two variables that were considered uncertain and could potentially affect the radiative heat transfer. Standard values for both of these emissivities are constant and set to 0.8 and as can be noted from Table 4.8 and 4.9 the outlet bed temperature is barely affected by a decrease or increase of the emissivities. The energy balance error for the bed emissivity from 0.2 to 0.6 is relatively large, however since the bed emissivity is estimated to be 0.8 the results show that the values for outlet bed temperature etc at emissivities 0.7 and 0.9 are not very different. This indicates that the bed temperature is not severely affected by the bed emissivity. It can also be noted that the radiative heat transfer is increased as the bed emissivity is increased, which is reasonable since the bed behaves more as a black body and absorbs more radiation when the emissivity is increased. When instead the inner wall emissivity is increased the radiation is slightly decreased. A potential reason for this could be that the walls do not reflect as much radiation to the bed as the inner wall emissivity is increased. Furthermore, the conduction decreases as the bed emissivity increases and the other way around for the inner wall emissivity. The explaination for this could be that as the bed absorbs more radiation, less radiation is reflected to the walls, which leads to lower wall temperature and thus lower heat transfer through conduction. When the inner wall emissivity is instead increased, the walls absorbs more radiation and thus the heat transfer through conduction is increased following the same argument.

Table 4.8: Outlet bed temperature, heat transfer mechanisms to the bed, heat losses and heat demand for varying bed emissivity

Bed emissivity	0.1	0.2	0.3	0.4	0.5	0.6	0.7	0.8	0.9	1
Outlet bed temp (°C)	1312	1312	1312	1312	1312	1312	1339	1343	1345	1348
Radiation (MW)	2.69	5.09	7.24	9.15	10.91	12.49	13.34	14.36	15.50	16.46
Convection (MW)	7.67	7.53	7.43	7.32	7.24	7.17	6.84	6.72	6.64	6.56
Conduction (MW)	22.68	21.18	19.92	18.73	17.73	16.83	15.41	14.57	13.83	13.19
Total heat to bed (MW)	33.05	33.79	34.58	35.20	35.88	36.50	35.59	35.75	35.97	36.21
Outer heat losses (MW)	1.64	1.64	1.63	1.63	1.63	1.62	1.63	1.63	1.63	1.63
Heat to gas (MW)	22.90	22.90	22.90	22.90	22.90	22.90	22.90	22.90	22.90	22.90
Energy balance error (MW)	0.59	1.32	2.11	2.72	3.39	4.00	0.39	0.16	0.13	0.14
Total heat demand (MW)	57.59	58.33	59.12	59.74	60.41	61.03	60.12	60.29	60.50	60.74

Table 4.9: Outlet bed temperature, heat transfer mechanisms to the bed, heat losses and heat demand for varying inner wall emissivity

Inner wall emissivity	0.4	0.5	0.6	0.7	0.8	0.9	1
Outlet bed temp (°C)	1311	1311	1311	1341	1343	1345	1346
Radiation (MW)	15.93	15.71	15.43	14.62	14.46	14.40	14.31
Convection (MW)	12.01	13.28	14.06	14.13	14.57	14.95	15.22
Conduction (MW)	12.01	13.28	14.06	14.13	14.57	14.95	15.22
Total heat to bed (MW)	35.31	36.29	36.67	35.56	35.75	36.02	36.13
Outer heat losses (MW)	1.59	1.60	1.61	1.62	1.63	1.63	1.64
Heat to gas (MW)	22.90	22.90	22.90	22.90	22.90	22.90	22.90
Energy balance error (MW)	3.13	4.03	3.32	0.26	0.16	0.19	0.11
Total heat demand (MW)	59.81	60.79	61.18	60.09	60.29	60.56	60.68

5
Conclusion

The results obtained from the simulations performed during this project indicate that there is good potential for a thermal plasma to replace the fossil fueled burners currently used in the rotary kiln for cement production. Various methods to affect the heat transfer mechanisms to the bed material has been investigated. Some of these methods prove to be more successful than others for reaching a sufficiently high temperature of the outlet bed. Increasing the temperature of the plasma itself as well as incorporating particles to help with the radiative heat transfer are methods which are worth investigating further. Also, preheating the inlet gas has the potential to work in combination with other methods to reach the desired outlet bed temperature. Furthermore, the sensitivity analysis showed that the results are rather robust, if the estimated values of the emissivities would be higher or lower than predicted.

Validation of the simulations by measurements and tests on pilot-scale or full scale kilns should probably be one of the steps to further assure that the results are trustworthy.

5. Conclusion

6
Further research suggestions

Measurements performed on experimental setups seem reasonable in order to validate the model and the assumptions made in the model. For example measurements on the temperature profile for the plasma would be beneficial to become more certain about the accuracy of that assumption. Furthermore, it should be investigated how the dissociation of carbon dioxide due to the high temperatures in the kiln could be incorporated into the model. Also, the impact on the heat transfer from incorporating different particles, such as calcium carbonate, should be further examined.

6. Further research suggestions

Bibliography

[1] UN, "The Paris Agreement - main page," 2016. [Online]. Available: https://unfccc.int/process-and-meetings/the-paris-agreement/the-paris-agreement

[2] E. Benhelal, G. Zahedi, E. Shamsaei, and A. Bahadori, "Global strategies and potentials to curb CO2 emissions in cement industry," 2013.

[3] IEA, "Cement," 2021. [Online]. Available: https://www.iea.org/reports/cement

[4] M. Schneider, M. Romer, M. Tschudin, and H. Bolio, "Cement and Concrete Research Sustainable cement production — present and future," *Cement and Concrete Research*, vol. 41, no. 7, 2011.

[5] Cementa, "Nollvision för koldioxid." [Online]. Available: https://www.cementa.se/sv/nollvision2030

[6] S. Nie, J. Zhou, F. Yang, M. Lan, J. Li, Z. Zhang, Z. Chen, M. Xu, H. Li, and J. G. Sanjayan, "Analysis of theoretical carbon dioxide emissions from cement production: Methodology and application," *Journal of Cleaner Production*, vol. 334, p. 130270, 2022. [Online]. Available: https://www.sciencedirect.com/science/article/pii/S0959652621044358

[7] Cementa, "Det här är CCS." [Online]. Available: https://www.cementa.se/sv/det-har-ar-ccs

[8] N. Venkatramani, "Industrial plasma torches and applications," *Current Science*, vol. 83, no. 3, 2002.

[9] A. Gunnarsson, "Radiative Heat Transfer in Suspension-Fired Systems." *THESIS FOR THE DEGREE OF DOCTOR OF PHILOSOPHY*, 2019. [Online]. Available: https://research.chalmers.se/publication/511425/file/511425_Fulltext.pdf

[10] Cementa AB, "Cementproduktion steg-för-steg," 2022. [Online]. Available: https://www.cementa.se/sv/cementproduktion-steg-f%C3%B6r-steg

[11] G. Habert, "Assessing the environmental impact of conventional and 'green' cement production," in *Eco-Efficient Construction and Building Materials: Life Cycle Assessment (LCA), Eco-Labelling and Case Studies*, 2013.

[12] B. Wilhelmsson, C. Kollberg, J. Larsson, J. Eriksson, and M. Eriksson, "CemZero - a feasibility study evaluating ways to reach sustainable cement production via the use of electricity," 12 2018.

[13] A. R. Nielsen, "Combustion of large solid fuels in cement rotary kilns," Ph.D. dissertation, 2012.

[14] P. Taylor and S. Pirzada, "Thermal Plasma Processing of Materials: A Review," *Advanced Performance Materials*, vol. 1, pp. 35–50, 2 1994.

[15] Rudolfensis, "File:Non-transferred DC plasma torch.png," Licensed under the Creative Commons Attribution-ShareAlike 3.0 Unported (CC BY-SA 3.0),

https://creativecommons.org/licenses/by-sa/3.0/deed.en, 5 2012. [Online]. Available: https://commons.wikimedia.org/wiki/File:Non-transferred_DC_plasma_torch.png#filelinks

[16] M. Zhukov and I. Zasypkin, "Thermal plasma torches - Design, Characteristics, Applications," 2006.

[17] S. L. Camacho, "Industrial-worthy plasma torches: State-of-the-art," *Pure and Applied Chemistry*, vol. 60, no. 5, pp. 619–632, 1988. [Online]. Available: https://doi.org/10.1351/pac198860050619

[18] A. Gunnarsson, K. Andersson, B. R. Adams, and C. Fredriksson, "Full-scale 3D-modelling of the radiative heat transfer in rotary kilns with a present bed material," *International Journal of Heat and Mass Transfer*, vol. 147, 2 2020.

[19] A. Gunnarsson, D. Bäckström, R. Johansson, C. Fredriksson, and K. Andersson, "Radiative Heat Transfer Conditions in a Rotary Kiln Test Furnace Using Coal, Biomass, and Cofiring Burners," *Energy and Fuels*, vol. 31, no. 7, pp. 7482–7492, 7 2017.